Static and Dynamic Response Analysis of Raman Injection Quantum Cascade Laser Using Circuit Level Modeling

Hossein Reza Yousefvand, Vahid Ahmadi, *Senior Member, IEEE*, and Kamyar Saghafi

***Abstract*—In this paper a new approach for modeling of Raman quantum cascade lasers (QCLs) is presented which integrates electrical, optical and Raman effects. The equivalent circuit model of laser by employing simplified two-level rate equations of pump and Raman regions is developed. The total equivalent circuit is composed of pump laser circuit coupled to Raman laser circuit which models the behaviors of each component and whole device. By using the presented model the static and dynamic performances of laser for different parameters are investigated. The results of simulation show that the main characteristics of laser such as threshold current, quantum efficiency, output power and modulation response are affected by photon lifetime and variation of population inversion conditions. Static results of model agree favorably with experimental data from devices reported in the literatures.**

***Index Terms*—Circuit model, nonlinear optics, pump laser, quantum cascade laser, Raman laser, rate equations.**

I. Introduction

QUANTUM cascade (QC) lasers are midto-far infra-red semiconductor lasers, where photons are generated by radiative intersubband transitions in quantum wells [2]. Compared with conventional semiconductor lasers based on the interband transition between electrons in conduction band and holes in the valence band, QCLs rely on the intersubband transition between conduction subbands. Because of the characteristics of the intersubband transition, QCLs are expected to have advantages over conventional semiconductor lasers such as a narrow and symmetric gain spectrum and less temperature dependence of the threshold current [3]. In the past few years, the nonlinear optical properties in the low-dimensional semiconductor quantum systems, such as quantum wells, quantum wires and quantum dots, have attracted much attention both in practical applications and in theoretical research. Intersubband transitions in asymmetric coupled quantum wells can produce large nonlinear optical nonlinearities based on intersubband transitions and QCLs has several advantages [5].

Manuscript received May 04, 2010; revised August 17, 2010; accepted September 05, 2010. Date of publication September 20, 2010; date of current version October 27, 2010. This work was supported in part by the Iran Telecommunication Research Centre (ITRC).

H. R. Yousefvand is with the Department of Electrical Engineering Science and Research Branch, Islamic Azad University, Tehran 1477893855, Iran (e-mail: hossein.usef@srbiau.ac.ir).

V. Ahmadi is with the School of Electrical and Computer Engineering, Tarbiat Modares University, Tehran 14115-143, Iran (e-mail: v_ahmadi@modares.ac.ir).

K. Saghafi is with the Department of Electrical Engineering, Shahed University, Tehran 3319118651, Iran (e-mail: saghafi@shahed.ac.ir).

Digital Object Identifier 10.1109/JLT.2010.2077731

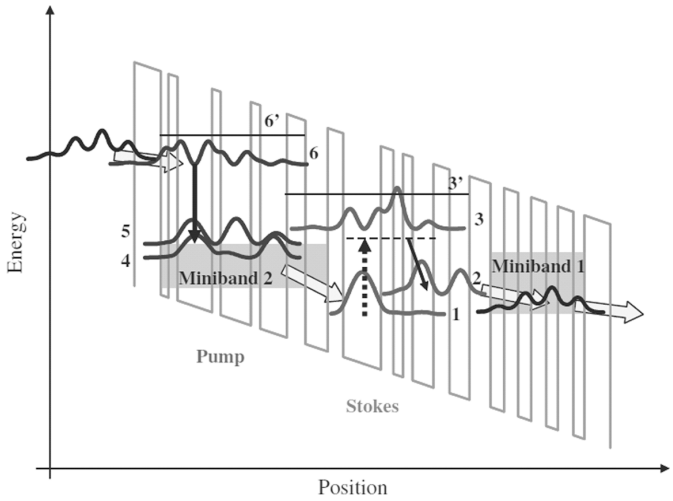

Fig. 1. Schematic structure of RI-QCL. The energy barriers (0.52 eV) are made of $Al_{0.48}In_{0.52}$ As and the quantum wells of $Ga_{0.47}In_{0.53}$ As.

Integrated QCLs can provide high optical power densities which make very effective pump sources and, at the same time, good overlap between pump modes and the nonlinear region is obtained. Recently the generation of sum frequency, second harmonic and third harmonic in QCLs have been reported [6]–[8]. Stimulated Raman scattering is a third-order nonlinear optical process which enables generation of optical gain at a frequency shifted from the incident radiation by an amount corresponding to the frequency of an internal oscillation of the material [11]. The wavelength shift between the fundamental and the Raman emission is determined by resonance frequency of the internal oscillations which can be due to vibrational (phonon), rotational, plasmonic, or electronic resonances [1]. This effect is the basis for a broad class of tunable sources known as optically-pumped Raman lasers [12]. In general, these sources have only small gain ($\sim 10^{-9}$ cmW $^{-1}$) and therefore require external pumping with powerful lasers, which limits their applications.

To circumvent these limitations of traditional Raman laser, Raman injection quantum cascade laser (RI-QCL) with a structure shown in Fig. 1 has been developed [9]. RI-QCL is based on triply resonant stimulated Raman scattering between quantum confined states within the active region of a QCL that serves as an internal optical pump. The main idea of RI-QCL is to monolithically integrate active laser medium and the nonlinear medium in such a way that the laser field could serve as an intra-cavity optical pump for the desired nonlinear optical interaction [18]. The active nonlinear systems support both laser action and, at the same time, nonlinear self-conversion of laser

light into coherent radiation at different frequencies. The nonlinear section, a coupled quantum well containing a desired set of intersubband transitions, is incorporated into an active region of a QCL for intersubband transitions. RI-QCL is driven electrically without any external laser pump and Raman lasers. It combines the advantages of nonlinear optical devices and semiconductor injection lasers leading to a new class of compact midand far-infrared light sources with order of magnitude enhancement of Raman gain, high conversion efficiency and low threshold [1].

Clearly, in order to effectively design optoelectronic applications incorporating Raman injection (RI) lasers, appropriate models are required. To our knowledge, for the first time, this paper describes a circuit level implementation of RI-QCL to analyze the static and dynamic performances of laser for different parameters. The results of physically based circuit model of Raman injection laser are compared with experimental measurements. The laser parameters are determined from lasers fabricated in [9]. The paper is organized as follows. In Section II, the model of the RI-QCL is introduced. In Section III, the circuit model implementation is described, and results are discussed in Section IV. Finally, conclusion is brought in Section V.

II. Model Development

Our model which describes the carrier dynamics of RI-QCL is based on the experimental works in [9]. In this injection-pumped Raman laser the fundamental and the Raman radiations are both generated by intersubband electronic transitions in the very same active region of a QCL.

The schematic structure of active region of a resonant RI-QCL that integrates the fundamental laser cascade $6 \rightarrow 5 \rightarrow 4$ and transitions $1 \rightarrow 3 \rightarrow 2 \rightarrow 1$ for Raman Stokes lasing is illustrated in Fig. 1. In our model the analysis splits in two sequential steps. At first, the behavior of pump (the first part of the structure) which acts as a pump to the Raman stage is modeled by three coupled rate equations. Then, the incident photon of energy $\hbar\omega_{\rm p}$, produced by the previous step, is converted into a Stokes photon of energy $\hbar\omega_{\rm s}$. This step is modeled by three coupled rate equations in Raman region.

The carriers are injected into level 6, i.e., the upper pump laser level, by resonant tunneling. After the radiative laser transition $(6 \rightarrow 5)$, the carriers relax into level 4 by the emission of a longitudinal-optical phonon $(5 \rightarrow 4)$ and tunnel through the barrier into the Raman region. From there, the electrons are injected into the lower Raman laser level. The pump region of each stage consists of vertical transition of coupled wells active region, used in the design of state-of-the-art midinfrared QC lasers and suitably modified for optimum coupling to the Raman region [10]–[13]. A simplified dynamic diagram of population in pump region is shown in Fig. 1. The system of rate equations for electron numbers $\rm N_6$ and $\rm N_5$ in levels 6 and 5, and the photon number $\rm N_P$ in the pump region can be written as [14]

$$\frac{dN_6}{dt} = \eta_1 \frac{I}{q} - \frac{N_6}{\tau_6} - \Gamma_P \frac{c'\sigma_{65}}{V} \times (N_6 - N_5) N_P \tag{1}$$

$$\frac{dN_5}{dt} = (1-\eta_1)\frac{I}{q} - \frac{N_5}{\tau_{54}} + \frac{N_6}{\tau_{65}} + \Gamma_P \frac{c'\sigma_{65}}{V}(N_6 - N_5) N_P \tag{2}$$

$$\frac{dN_P}{dt} = -\frac{N_P}{\tau_P} + \Gamma_P N \frac{c'\sigma_{65}}{V} \times (N_6 - N_5) N_P \tag{3}$$

where η_1 is the injection efficiency into the upper laser state, q is the electronic charge, I is the electron injection current tunneling into level 6, $\rm V = N \cdot W \cdot L \cdot L_t$ is volume of the cavity, W and L are the width and length of the cavity, respectively, and $\rm L_t$ is the length of a single stage of the cascade laser structure, N is the number of stages, $\acute{c} = \rm c_0/n_{1eff}$ is the velocity of light in medium ($\rm n_{1eff}$ is the effective refractive index of pump mode), τ_6 is the total lifetime of electrons in level 6, τ_{ij} ($\rm i = 6, 5$ and $\rm j = 5, 4$) is the phonon scattering time between levels i and j. The photon lifetime τ_P inside the cavity can be expressed as $\tau_{\rm P}^{-1} = \acute{c}(\alpha_{\rm w} + \alpha_{\rm m})$ where $\alpha_{\rm w}$ is the waveguide loss of the cavity and $\alpha_{\rm m}$ is the mirror loss, given by $\alpha_{\rm m} = -\ln(\rm R_1 R_2)/(2L)$. $\rm R_1$ and $\rm R_2$ are reflectivities of facets 1 and 2, respectively. $\Gamma_{\rm P}$ and σ_{65} are the pump mode confinement factor and the stimulated emission cross section, respectively. The parameter σ_{65} is given by [14]

$$\sigma_{65} = \frac{4\pi e^2 z_{65}^2}{n_{1\rm eff}\varepsilon_0 \lambda_{\rm Ph}(2\gamma_{65})} \tag{4}$$

where $\rm ez_{65}$ is the dipole matrix element, $\lambda_{\rm ph}$ is the pump emission wavelength, ε_0 is the vacuum permittivity, $2\gamma_{65}$ is the FWHM which is mainly due to longitudinal-optical phonon scattering. In (3), spontaneous emission has been neglected and we have assumed for simplicity that all gain stages are identical. In general case, transfers towards satellite valleys should also be considered and X valleys states should be treated in a similar way as Γ valley states [14]. However, extensive investigations by Gao *et al.* [15] indicate that these contributions are small for $\rm Al_{0.48}$ In $_{0.52}\rm As/Ga_{0.47}In_{0.53}As$ QCLs, and therefore we neglect them for the sake of simplicity.

Regarding the Raman process sketched in Stokes part of Fig. 1 the internal oscillations in a medium correspond to the transition between states 1 and 2. The incident light with energy of $\hbar\omega_{\rm P}$ (energy of pump photon) is converted into a signal with $\hbar\omega_{\rm S}$ energy, called Stokes radiation. Both frequencies are usually strongly detuned from other higher-lying states to avoid strong first-order absorption. In this case, only two-photon transitions between state 1 and 2 mediated by an intermediate virtual state may occur [9]. The time dependent populations of subband 1 and 2, neglecting the third-level population, and number of Stokes photons, self-consistent rate equations can be written as [16]

$$\frac{dN_1}{dt} = \eta_2 \frac{I}{q} - \frac{N_1}{\tau_1^{\rm eff}} + \frac{N_2}{\tau_{21}} - K_1 \frac{\Gamma_S}{V}\frac{d^2\sigma}{d\omega_s d\Omega} \times (N_1 - N_2) N_P N_S \tag{5}$$

$$\frac{dN_2}{dt} = (1-\eta_2)\frac{I}{q} - \frac{N_2}{\tau_2^{\rm eff}} + \frac{N_1}{\tau_{12}} + K_1 \frac{\Gamma_S}{V}\frac{d^2\sigma}{d\omega_s d\Omega} \times (N_1 - N_2) N_P N_S \tag{6}$$

$$\frac{dN_S}{dt} = -\frac{N_S}{\tau_C} + K_2 N \frac{\Gamma_S}{V}\frac{d^2\sigma}{d\omega_s d\Omega} \times (N_1 - N_2) I_{\rm Pump} N_S \tag{7}$$

where

$$K_1 = \frac{8\pi^3 c^4}{\omega_S^2 n_{2\rm eff}^3} \tag{8}$$

$$K_2 = \frac{4\pi^3 c^3}{\omega_S^2 \hbar\omega_P n_{2\rm eff}^3} \tag{9}$$

$$I_{\mathrm{Pump}} = \frac{cN_P\hbar\omega_P}{V_r n_{1\mathrm{eff}}} \tag{10}$$

$$\frac{d^2\sigma}{d\omega_S d\Omega} = K_3 Z_{32}^2 Z_{31}^2 \left[\frac{\hbar\Gamma}{\delta^2+\Gamma^2}\right]. \tag{11}$$

In (5)–(11), $\mathrm{V_r} = \mathrm{W}\cdot\mathrm{L}\cdot\mathrm{L_s}$ is the volume of the Raman region, $\mathrm{L_s}$ is the length of the Raman region in a single stage of the cascade laser structure. $\mathrm{N_1}$ and $\mathrm{N_2}$ are the electron populations in subband 1 and 2, $\mathrm{N_S}$ is the Raman photon number, η_2 is the injection efficiency into lower state of the Raman region. The relaxation times of electrons between the subbands are denoted as τ_{21} (from 2 to 1), τ_{12} (from 1 to 2), τ_1 $^{\mathrm{eff}}$ (effective relaxation time out of 1), τ_2 $^{\mathrm{eff}}$ (effective relaxation time out of 2) and τ_{C} (cavity life-time of Stokes photon). $\mathrm{n_{2eff}}$ is the effective refractive index of Stokes mode, Γ_{S} is the Stokes mode confinement factor, $\mathrm{I_{Pump}}$ is pump intensity, $\delta(=\mathrm{E_{31}}-\hbar\omega_{\mathrm{P}})$ denotes the detuning of pump laser and Γ is the line width of intersubband transition. $\mathrm{Z_{ij}(i=3, j=2, 1)}$ is the dipole matrix element defined as $\mathrm{Z}_{ij} = \langle\psi_{\mathrm{i}}|\mathrm{z}|\psi_{\mathrm{j}}\rangle$, where ψ_{i} is the envelope wave function of ith subband. $d^2\sigma/d\omega_s d\Omega$ is the spectral differential scattering cross section and $\mathrm{K_3}$ is a constant already defined in [16].

III. Circuit Model Implementation

In this work we develop a circuit model for RI-QCLs in order to analyze the characteristics of the device in HSPICE. Proportional to the carrier and photon numbers, we define new variables of $\mathrm{V_{Ni}}$ and $\mathrm{V_{P,S}}$ scaled with the arbitrary constants $\mathrm{z_N}$ and k, and to obtain better convergence the square of $\mathrm{V_{P,S}}$ is used

$$N_i = z_n \cdot V_{\mathrm{Ni}}|_{Z_n\approx 10^{15}} \tag{12}$$

$$N_{P,S} = \left.\frac{(V_{P,S}+\delta)^2}{k}\right|_{k\approx 1.5\cdot 10^{-19}} \quad \delta \geq 0 \tag{13}$$

where $\mathrm{N_i}$ and $\mathrm{N_{P,S}}$ are carrier and photon numbers, respectively, $\mathrm{V_{Ni}}$ is correspond to voltage over node $\mathrm{N_i}$ and $\mathrm{V_{P,S}}$ is correspond to voltage over node p and s respectively of circuit that is shown in Fig. 2. Substituting (12)–(13) into (1)–(7) and applying proper operations, we obtain normalized-rate equations which can be mapped directly into a circuit for RI-QCL illustrated in Fig. 2. By proper selection of elements and applying Kirchhoff current law to nodes of circuit illustrated in Fig. 2 the normalized-rate equations of RI-QCL are obtained. Accordingly, the normalized-carrier rate (1) is modeled with the capacitor $\mathrm{C_{N6}}$, resistor $\mathrm{R_{N6}}$, and the nonlinear current source $\mathrm{G_{N65}}$ where

$$C_{N6} = qz_n \tag{14}$$

$$R_{N6} = \frac{\tau_6}{qz_n} \tag{15}$$

$$G_{N65} = qz_n \cdot \frac{c'\sigma_{65}\Gamma_P}{kV}(V_{N6}-V_{N5}) \times (V_P+\delta)^2 \tag{16}$$

In the same way, the normalized-carrier rate (2) is modeled with the capacitor $\mathrm{C_{N5}}$, resistor $\mathrm{R_{N5}}$, and the nonlinear current sources $\mathrm{G_{N65}}$ and G_{N5} where

$$C_{N5} = qz_n \tag{17}$$

$$R_{N5} = \frac{\tau_{54}}{qz_n} \tag{18}$$

$$G_{N5} = \frac{qz_n}{\tau_{65}}(V_{N6}) \tag{19}$$

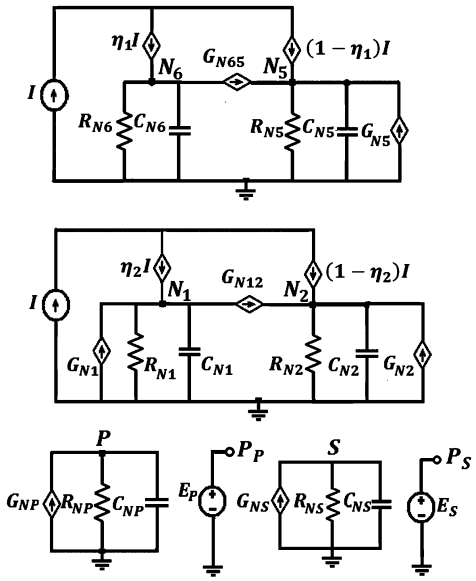

Fig. 2. Circuit-level implementation of RI-QC laser.

The normalized-photon rate (3) is modeled with capacitor $\mathrm{C_{NP}}$, resistor $\mathrm{R_{NP}}$, and the nonlinear current source $\mathrm{G_{NP}}$ where

$$C_{NP} = 2\tau_{\mathrm{P}} \tag{20}$$

$$R_{NP} = 1 \tag{21}$$

$$G_{NP} = z_n\frac{\Gamma_P}{V}c'\sigma_{65}\tau_P(V_{N6}-V_{N5}) \times (V_{\mathrm{P}}+\delta)-\delta. \tag{22}$$

Similarly, capacitor $\mathrm{C_{N1}}$, resistor $\mathrm{R_{N1}}$, and the nonlinear current sources $\mathrm{G_{N1}}$ and $\mathrm{G_{N12}}$ model the normalized-carrier rate (5), where

$$C_{N1} = qz_n \tag{23}$$

$$R_{N1} = \frac{\tau_1^{\mathrm{eff}}}{qz_n} \tag{24}$$

$$G_{N1} = \frac{qz_n}{\tau_{21}}(V_{N2}) \tag{25}$$

$$G_{N12} = qz_n \cdot \frac{K_1\Gamma_S}{k^2V}\frac{d^2\sigma}{d\omega_s d\Omega}(V_{N1}-V_{N2}) \times (V_P+\delta)^2(V_S+\delta)^2. \tag{26}$$

The normalized-carrier rate (6) is modeled with capacitor $\mathrm{C_{N2}}$, resistor $\mathrm{R_{N2}}$ nonlinear current sources $\mathrm{G_{N2}}$ and $\mathrm{G_{N12}}$ where

$$C_{N2} = qz_n \tag{27}$$

$$R_{N2} = \frac{\tau_2^{\mathrm{eff}}}{qz_n} \tag{28}$$

$$G_{N2} = \frac{qz_n}{\tau_{12}} \times V_{N1}. \tag{29}$$

Finally, the normalized-photon rate (7) is modeled with capacitor $\mathrm{C_{NS}}$, resistor R_{NS}, and nonlinear current source G_{NS} that

$$C_{NS} = 2\tau_C \tag{30}$$

$$R_{NS} = 1 \tag{31}$$

$$G_{NS} = z_n\tau_C\frac{K_4N\Gamma_S}{kV}\frac{d^2\sigma}{d\omega_s d\Omega}(V_{N1}-V_{N2}) \times (V_{\mathrm{P}}+\delta)^2(V_S+\delta)-\delta \tag{32}$$

TABLE I
PARAMETERS USED IN RI-QC LASER CIRCUIT MODEL [9], [16]

Symbol	Description	Value
τ_6	Total lifetime of electron in level 6	1.16ps
τ_{65}	Phonon scattering time between levels 6 and 5	2.1ps
τ_{54}	Phonon scattering time between levels 6 and 5	0.3ps
τ_{1eff}	Effective relaxation time of level 1	0.903ps
τ_{2eff}	Effective relaxation time of level 2	0.223ps
τ_{21}	2 to 1 relaxation time	0.226ps
τ_{12}	2 to 1 relaxation time	10.11ps
τ_p	Pump photon lifetime in the cavity	5.77ps
τ_c	Stokes photon lifetime in the cavity	9.57ps
η_1	Injection efficiency into level 6	0.75
η_2	Injection efficiency into level 1	0.85
n_{1eff}	Effective refractive index of pump mode	3.27
n_{2eff}	Effective refractive index of Stokes mode	3.2
Γ_p	Confinement factor of pump mode	0.32
Γ_s	Confinement factor of Stokes mode	0.16
Γ	Line width of intersubband transition	5meV
δ	Detuning	13meV
W	Width of the cavity	34μm
L	Length of the cavity	2 mm
L_p	Length of pump region in a single stage	45 nm
L_s	Length of Stokes region in a single stage	10 nm
λ_p	Pump emission wavelength	6.9μm
λ_s	Stokes emission wavelength	8.9μm
K_3	Constant	0.15×10^{-6}
N	Number of stages	30
T	Temperature	77 K
η_o	Output-power coupling coefficient	0.5
Z_{31}	3 to 1 dipole matrix element	1.23 nm
Z_{32}	3 to 2 dipole matrix element	1.31 nm
Z_{65}	6 to 5 dipole matrix element	1.7 nm

where

$$K_4 = \frac{4\pi^3 c^4}{\omega_S^2 n_{2\text{eff}}^3 n_{1\text{eff}} V_r}. \tag{33}$$

Since we are mainly interested in the output light power we use a voltage controlled voltage source ($\mathrm{E_P}$) to calculate the output power as:

$$P_{P,S} = \frac{(V_{P,S}+\delta)^2}{k\tau_{P,C}}\eta_{p,s}\hbar\omega_{p,S}. \tag{34}$$

$\mathrm{P_P}$ and $\mathrm{P_S}$ are terminals whose nodes voltages model the output power of pump and Stokes laser, respectively.

IV. RESULTS AND DISCUSSION

A. Steady-State Analysis

We have chosen some typical values of the parameters for RI-QCL shown in Table I, which match closely for the devices reported in [9], [14], [16]. Fig. 3(a) shows the variation of steady state optical output power versus bias currents when the pump photon life time τ_{P} changes from 1 to 9 ps for $\xi = 0.15$, where ξ is equal to ratio of τ_{54}/τ_6, τ_{54} is the lifetime determining the removal rate of the carriers from the lower subband and τ_6 is the carrier lifetime of the upper subband given by $\tau_6^{-1} = \tau_{65}^{-1} + \tau_{64}^{-1}$. As shown in the figure, the threshold current increases for longer photon lifetimes. In Fig. 3(b) the effect of ξ on the L–I characteristic is shown. For larger values of ξ parameter when photon lifetime has a typical value, the carrier lifetime increases and the total rate of population inversion reduces, which leads to the degradation of quantum efficiency and rising of the threshold current of pump laser.

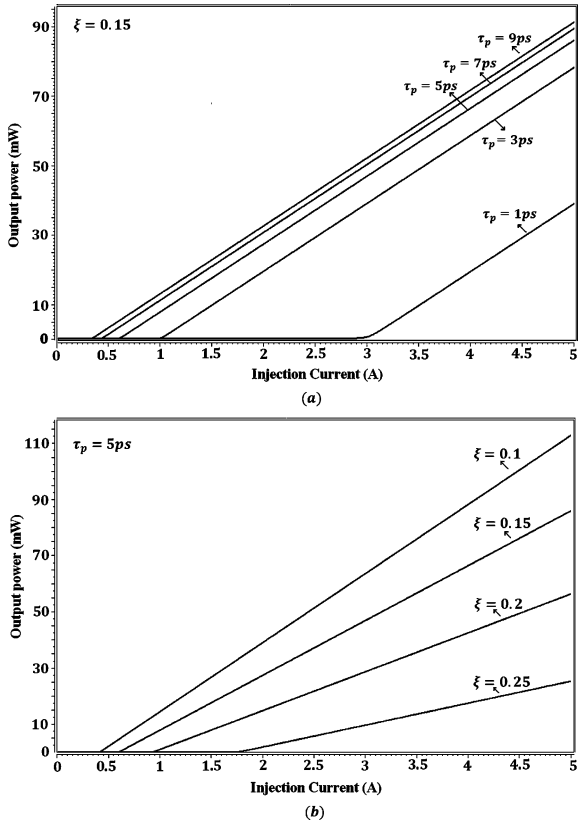

Fig. 3. Output power of pump laser versus injected current. (a) $\xi = 0.15$ and different values of pump photon lifetime, $\tau_{\mathrm{P}} = 1, 3, 5, 7$ and 9 ps. (b) $\tau_p = 6$ ps and $\xi = 0.1, 0.15, 0.2$ and 0.25.

Fig. 4(a) shows the light–current characteristics of Stokes laser when the photon lifetime τ_{P} changes from 1 to 9 ps for $\xi = 0.15$ and Stokes lifetime $\tau_{\mathrm{c}} = 9$ ps. It can be seen from Fig. 4(a), for longer pump photon lifetimes the threshold current of Stokes laser decreases and quantum efficiency enhances. In Fig. 4(b), the effect of ξ which corresponds to population inversion rate in pump laser, on L–I characteristic of Stokes laser is shown. The Stokes output power which is proportional to intensity of pump power deteriorates with increase of ξ parameter. This leads to degradation of quantum efficiency and higher threshold current of Stokes laser. Fig. 4(c) shows the light–current characteristics of Stokes laser when ξ and τ_{P} have typical values and the Stokes photon lifetime τ_{C} changes from 5 to 13 ps. This figure shows that longer Stokes photon lifetime causes a lower threshold current and greater slope efficiency of Stokes laser. The simulated and experimental L-I curves are compared in Fig. 5. All parameters used in simulation and experiment have typical values shown in Table I. As can be observed, Fig. 5 shows excellent agreement between threshold currents for simulated and experimental LI data. However, the simulated curves show a bit larger slope efficiencies at higher output power with no rollover at 55 mW. Most probably, fundamental laser deteriorates owing to misalignment in the resonant electron tunneling through the cascade, which is a common problem with QCLs far above threshold [17].

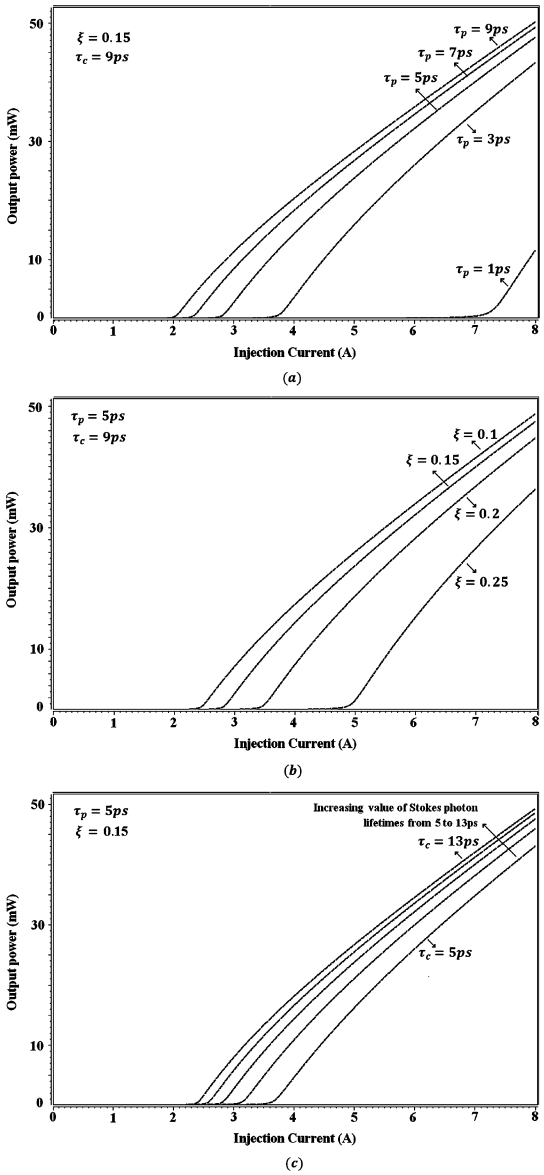

Fig. 4. Output power of Stokes laser versus injected current. (a) $\xi = 0.15$, Stokes photon lifetime $\tau_{\rm C} = 9$ ps and different values of pump photon lifetime $\tau_p = 1, 3, 5, 7$ and 9 ps. (b) $\tau_{\rm P} = 5$ ps, $\tau_{\rm c} = 9$ ps and $\xi = 0.1, 0.15, 0.2, 0.25$. (c) $\xi = 0.15$, $\tau_{\rm P} = 5$ ps with different values of Stokes photon lifetime $\tau_{\rm c} = 5, 7, 9, 11$ and 13 ps.

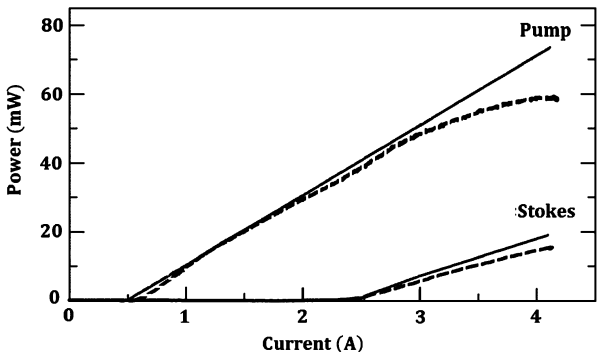

Fig. 5. Comparison of measured (dash line) and simulated (solid lines) LI curves for the device reported in [9].

B. Transient Characteristic Analysis

Examples of transient analysis using the presented model for pump and Stokes lasers are plotted in Figs. 6, 7 and 8. The transient curves are the output power of the laser in response to an input current (1 ns pulse) varying between 0.5 and 4 A with 1 ps rise and fall times. In Fig. 6(a) the transient response of pump laser for various pump photon lifetime $\tau_{\rm P}$, is shown. As we can see, output power of pump laser increases with $\tau_{\rm P}$. By increasing $\tau_{\rm P}$ from 1 to 9 ps the rise time, $t_{\rm r}$, changes from 15 to 23 ps, and the fall time, $t_{\rm f}$, changes from 3.5 to 35 ps. In Fig. 6(b), the effect of ξ parameter on the output power is investigated. As explained for the results in Fig. 3(b), higher values of ξ, results in larger threshold current and lower output power of pump laser.

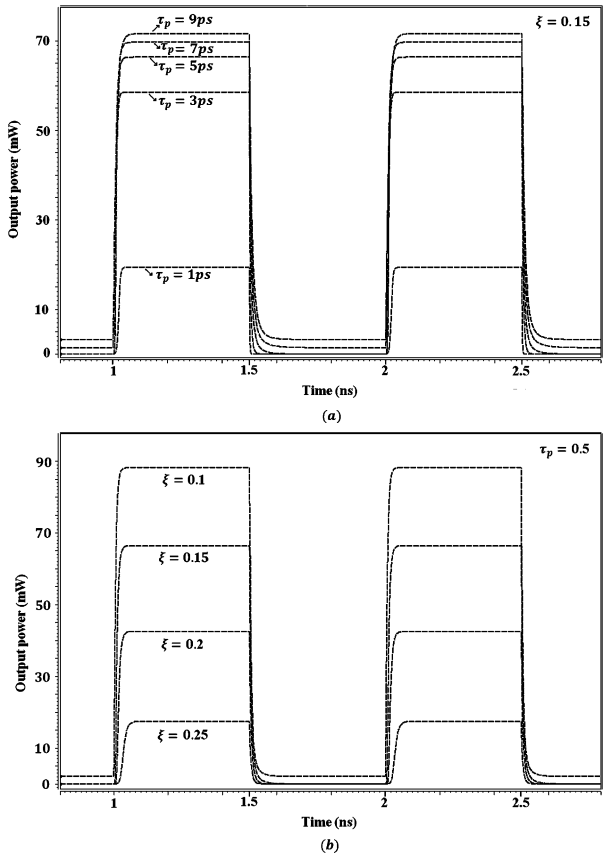

Fig. 6. Transient response of pump laser. (a) $\xi = 0.15$ and different values of pump photon lifetime $\tau_{\rm P} = 1, 3, 5, 7$ and 9 ps. (b) $\tau_{\rm P} = 5$ ps and $\xi = 0.1, 0.15, 0.2, 0.25$.

Fig. 7(a) shows the transient characteristics of Stokes laser when ξ and $\tau_{\rm P}$ have typical values and the Stokes photon lifetime $\tau_{\rm C}$ changes from 5 to 13 ps. By increasing $\tau_{\rm C}$, the rise time of Stokes output power reduces from 65 to 50 ps and fall time change from 13 to 32 ps. In Fig. 7(b) the effect of η_2, injection efficiency into lower Raman region state, on the transient response of Stokes laser is illustrated. As can be observed, total rate of stimulated Raman scattering increases with η_2 leading to greater Raman gain, and higher output power of Stokes laser.

The output power of pump and Stokes lasers with typical values of $\tau_{\rm P}, \tau_{\rm C}$ and ξ is shown in Fig. 8. The rise time and fall time of pump output power are 15 and 20 ps, respectively and the rise and fall times of Stokes output power are 45 and 23 ps, respectively. As expected in Figs. 6–8, in contrast to conventional semiconductor laser, the QCL has non-oscillating response for all output powers. The mechanism of damping oscillation can

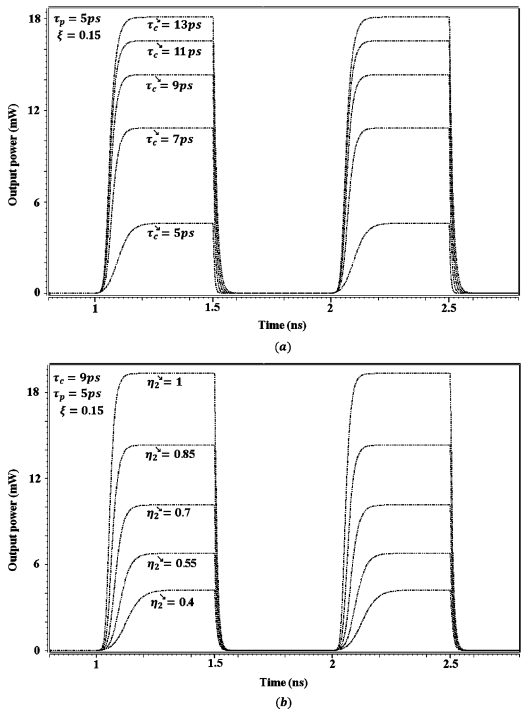

Fig. 7. Transient response of Stokes laser. (a) $\tau_{\rm p} = 5$ ps, $\xi = 0.15$ and different values of Stokes photon lifetimes $\tau_c = 5, 7, 9, 11$ and 13 ps. (b) $\tau_{\rm p} = 5$ ps, $\tau_{\rm c} = 9, \xi = 0.15$ and different values of injection efficiency into lower state $\eta_2 = 0.4, 0.55, 0.7, 0.85$ and 1.

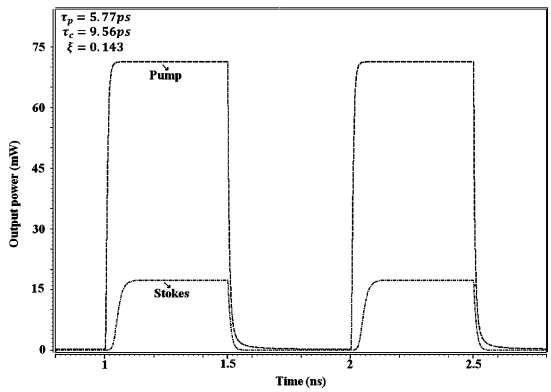

Fig. 8. Transient response of pump and Stokes lasers with typical values of ξ, $\tau_{\rm P}$ and $\tau_{\rm c}$.

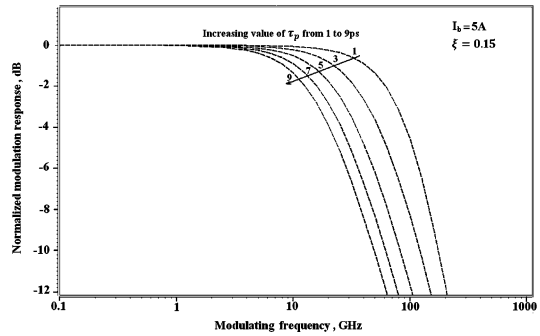

Fig. 9. Variation of normalized modulation response of pump laser with modulating frequency for different pump photon lifetimes $\tau_{\rm P} = 1, 3, 5, 7$ and 9 ps.

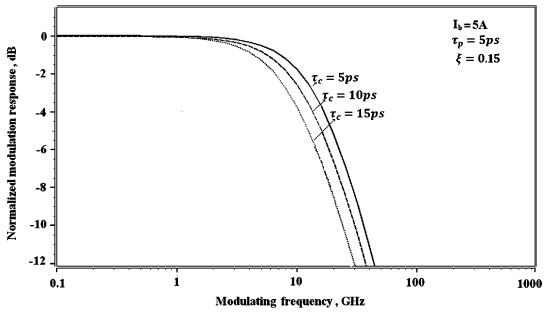

Fig. 10. Variation of normalized modulation response of Stokes laser with modulating frequency for different Stokes photon lifetimes $\tau_{\rm c} = 5, 10$, and 15 ps.

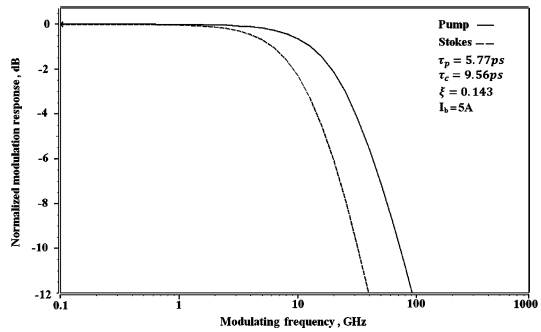

Fig. 11. Variation of the normalized modulation response of pump (dash line) and Stokes lasers (solid line) with typical values of ξ, $\tau_{\rm P}$ and $\tau_{\rm c}$.

be explained based on the rate equation as follows: in conventional semiconductor lasers, the increase of optical power brings about the decrease of distribution-reversed carrier density, reduction of the gain and optical power and oscillating response. In other words, photon population is damped by cavity losses, and carrier population is damped through its coupling to photon population. That is why the oscillation behavior appears at low powers. On the contrary, in QCL both electron and photon population are independently damped regardless of the output power [3].

C. Small Signal Analysis

In Fig. 9, the frequency response of pump laser for different values of pump photon lifetime is shown. Larger photon lifetime causes a degraded frequency.

Fig. 10 shows the small-signal frequency response of Stokes laser for three values of Stokes photon lifetime. Frequency response of pump and Stokes lasers for typical values given in [9], [16] is shown in Fig. 11. In all of Figs. 9–11, modulation response exhibits a non-resonant behavior of QCL that differs from in the conventional laser diodes. This can be explained from rate equations in the following way: the small-signal response around an operating point defined by a current injection $\rm I_0/e$ and photon number $\rm N_{Ph0}$ is derived from (1)–(3) [3]. Neglecting the second-level population, the modulus square of the frequency response is

$$|h(\omega')|^2 = \left[\omega'^4 + \omega'^2\left(\frac{\tau_P}{\tau_{\rm sti}} + 2\frac{\tau_P}{\tau_{65}} + \frac{\tau_P\tau_{\rm sti}}{\tau_{65}^2} - 2\right) + 1\right]^{-1} \quad (35)$$

where the normalized frequency is

$$\omega'^2 = \omega^2\tau_P\tau_{\rm sti} \quad (36)$$

and stimulated lifetime is defined as

$$\frac{1}{\tau_{\rm sti}} = \Gamma_P \frac{c'\sigma_{65}}{V} N_{\rm Ph0} \tag{37}$$

By setting $\tau_{65} = \infty$ in (35) the classical result for a conventional semiconductor laser is recovered, therefore the high-frequency rollover point does not depend on τ_{65}. When $\tau_{\rm sti} > \tau_{\rm P}$ the factor of the ω'^2 (parenthesis) is negative and resonance occurs. In contrast to conventional semiconductor lasers, in QCLs $\tau_{65} \approx 2$ ps. In (35) regardless of the value of $\tau_{\rm sti}$ as soon as $\tau_{\rm P} \geq \tau_{65}$ the factor of ω'^2 is positive and there is no resonance. In this work, $\tau_{\rm P}/\tau_{65} \approx 1$–$4$, so the frequency response is strongly damped. This damping is shown very clearly in Figs. 9–11. Since the photon lifetime and τ_{65} are typically a few picoseconds and the stimulated emission time is much less than 1ps, farther above laser threshold, one can predict that it is possible to modulate QCLs at frequencies more than hundred of gigahertz for higher injection currents corresponding to higher carrier and photon densities and lower stimulated emission time. This modulation bandwidth is more than one order of magnitude greater than that of the fastest diode lasers [3].

V. Conclusion

Based on two-level rate equations we have proposed an equivalent circuit model of RI-QCL for the analysis of the steady state and dynamic responses. By using the presented model the effects of various parameters on laser performance, such as threshold current, external quantum efficiency, output power and modulation response were investigated. Simulation results show that, the model can predict the effects of photon lifetime and population inversion condition on the laser performance. The dynamic analysis of model shows that regardless of output power, the QC-laser response does not exhibit any oscillation which is a different behavior compared with conventional lasers. It is shown that our static results agree favorably with experimental data reported earlier.

References

[1] A. Belyanin, F. Capasso, and M. Troccoli, *Intersubband Transition in Quantum Structures*, R. Paiella, Ed. New York: McGraw-Hill, 2006, ch. VI.

[2] J. Faist, F. Capasso, D. L. Sivco, C. Sirtori, A. L. Hutchinson, and A. Y. Cho, "Quantum cascade lasers," *Science*, vol. 264, pp. 553–556, 1994.

[3] J. Faist, F. Capasso, D. L. Sivco, and A. Y. Cho, *Quantum Cascade Lasers, in Intersubband Transition in Quantum Wells: Physics and Device Application II*, H. C. Liu and F. Capasso, Eds. New York: Academic, 2000, ch. VIII.

[4] M. K. Gumick and T. A. Detemple, "Synthetic nonlinear semiconductor," *IEEE J. Quantum Electron.*, vol. QE-19, no. 5, pp. 791–794, May 1983.

[5] A. Belyanin, F. Capasso, V. V. Kocharovsky, and M. O. Scully, "Infrared generation in low-dimensional semiconductor heterostructures via quantum coherence," *Phys. Rev. Lett.*, vol. 63, p. 053803, 2001.

[6] N. Owschimikow, C. Gmachl, A. Belyanin, V. Kocharovsky, D. L. Sivco, R. Colombelli, F. Capasso, and A. Y. Cho, "Resonant second order nonlinear process in quantum cascade lasers," *Phys. Rev. Lett.*, vol. 90, p. 043 902, 2003.

[7] O. Malis, A. Belyanin, C. Gmachl, D. L. Sivco, M. L. Peabody, A. M. Sergent, and A. Y. Cho, "Improvement of second-harmonic generation in quantum-cascade lasers with true phase-matching," *App. Phys. Lett.*, vol. 84, no. 15, pp. 2721–2723, 2004.

[8] T. S. Mosely, A. Belyanin, C. Gmachl, D. L. Sivco, M. L. Peabody, and A. Y. Cho, "Third harmonic generation in a quantum cascade laser with monolithically integrated resonant optical nonlinearity," *Opt. Exp.*, vol. 12, no. 13, pp. 2972–2976, 2004.

[9] M. Troccoli, A. Belyanin, F. Capasso, E. Cubukcu, D. L. Sivco, and A. Y. Cho, "Raman injection laser," *Nature*, vol. 433, pp. 845–848, 2005.

[10] J. Faist, D. Hafstetter, M. Beck, and T. Allen, "Bound-to-continuum and two-phonon resonance, quantum-cascade lasers for high duty cycle, high-temperature operation," *IEEE J. Quantum Electron.*, vol. 38, no. 6, pp. 533–546, Jun. 2002.

[11] R. W. Boyd, *Nonlinear Optics*, 2nd ed. San Diego, CA: Academic, 2003, pp. 528–531.

[12] Y. R. Shen, *The Principles of Nonlinear Optics*. Hoboken: Wiley, 1984.

[13] F. Capasso, C. Gmachl, R. Paiella, A. Tredicucci, A. L. Hutchinson, D. L. Sivco, J. N. Baillargeon, and A. Y. Cho, "New frontiers in quantum cascade lasers and applications," *IEEE Sel. Topics Quantum Electron.*, vol. 6, no. 6, pp. 931–947, Nov.–Dec. 2000.

[14] A. Hamadou, J. L. Thobel, and S. Lamari, "Modeling of temperature effects on the characteristics of midinfrared quantum cascade lasers," *J. Opt. Commun.*, vol. 281, pp. 5385–5388, 2008.

[15] X. Gao, D. Botez, and I. Knezevic, "X-valley leakage of GaAs-based midinfrared quantum cascade lasers: A Monte Carlo study," *J. Appl. Phys.*, vol. 101, p. 063101, 2007.

[16] S. M. Maung and S. Katayama, "Theory of intersubband Raman laser in modulation-doped asymmetric coupled double quantum wells," *J. Phys. Soc.*, vol. 73, pp. 2562–2570, 2004, Jpn.

[17] A. Belyanin, F. Xie, D. Liu, F. Capasso, and M. Troccoli, "Coherent nonlinear optics with quantum cascade structures," *J. Mod. Opt.*, vol. 52, no. 16, pp. 2293–2302, 2005.

[18] A. Belyanin, D. Liu, F. Xie, F. Capasso, and C. Gmachl, "Novel in-plane semiconductor lasers IV," in *Proc. SPIE*, C. Mermelstein and D. P. Bour, Eds., 2005, vol. 5738, pp. 98–108.

Hossein Reza Yousefvand received the B.S. degree in electronic engineering from Kashan University, Iran, in 2003 and M.S. degree in electrical engineering from Science and Research branch (SRB) of Islamic Azad University, Tehran, Iran, in 2005, where he is currently working towards the Ph.D. degree in electrical engineering on simulation and analysis of quantum cascade Raman amplifiers at SRB of Islamic Azad University.

Vahid Ahmadi (M'94–SM'10) received the Ph.D. degree in electronic engineering from Kyoto University, Kyoto, Japan in 1994.

He is a professor in Electronic Engineering at Tarbiat Modares University (TMU), Tehran, Iran. He was the head of the Electrical Engineering Department, TMU, 2006–2008. He is the member of the Founders-Board of Optics and Photonics Society of Iran. His current research interests include: quantum photonics devices, quantum optical modulators and amplifiers, optical microresonator active and passive devices, optical switches, slow light and photonic crystals.

Kamyar Saghafi received the Ph.D. degree in electronic engineering from Tarbiat Modares University, Tehran, Iran in 1994.

He is an Associate Professor in the Electronic Engineering at Department of Electrical Engineering, Shahed University, Tehran, Iran.